Journal of Alloys and Compounds 505 (2010) 400–403

Contents lists available at ScienceDirect

Journal of Alloys and Compounds

journal homepage: www.elsevier.com/locate/jallcom

Microstructure variations and their effect on the magnetic properties of a single die-cast $Nd_{60}Fe_{30}Al_{10}$ alloy rod

R.Ortega-Zempoalteca*, I. Betancourt, R. Valenzuela

Departamento de Materiales Metálicos y Cerámicos, Instituto de Investigaciones en Materiales, Universidad Nacional Autónoma de México, DF 04510, Mexico

ARTICLE INFO

Article history:
Received 23 February 2010
Received in revised form 14 April 2010
Accepted 24 April 2010
Available online 18 June 2010

PACS:
75.20.−g
75.30.−m
75.50.Kj
75.60.−d

Keywords:
Rare earth alloys
Amorphous materials
Magnetic measurements

ABSTRACT

Microstructure and magnetic properties for an as-quenched, single rod (3 mm diameter, 50 mm length) of $Nd_{60}Fe_{30}Al_{10}$ alloy obtained by copper mold casting technique, were characterized on three different zones along the rod length selected at the bottom, middle and upper part. The bottom part was in direct contact with an additional copper plate, while the upper part was located at the open side of the copper mold. A predominant amorphous microstructure was found at the bottom part of the rod for which maximum intrinsic coercivity of 3519 Oe was observed, while a magnetically decoupled composite structure was established at the opposite rod side, together with a noticeable reduction in coercivity (down to 3070 Oe). Results are interpreted on the basis of increasing crystalline volume fraction from bottom to the upper part of the alloy rod.

1. Introduction

Amorphous alloys based on RE–TM–Al (RE = rare earth, TM = transition metal) have been subject of research since 1988, when they were reported for the first time [1,2]. The glass forming ability (GFA) of these materials has the distinctiveness of being present for regions within phase diagrams with no deep eutectics points [3]. In particular, Nd–Al–TM (TM = Fe, Co, Ni, Cu) alloys with 60 at% Nd, 10–15 at% Al and 25–30 at% TM were described as systems able to be cast as bulk metallic glasses (BMG) in the form of rods of up to 6 mm of diameter by simple copper mold casting techniques [3]. Later on, the BMG $Nd_{90-x}Fe_xAl_{10}$ and $Pr_{90-x}Fe_xAl_{10}$ ($10 \leq x \leq 90$) series (of up to 7 mm diameter and 50 mm length) reported by Inoue and co-workers [4,5], exhibited a wide composition glass formation range for 10–65 at% Nd/Pr; 10–90 at% Fe and 20–50 at% Al. Additionally, they reported a surprisingly high intrinsic coercivity of 3462 Oe for the amorphous $Nd_{60}Fe_{30}Al_{10}$ sample and 3750 Oe for the glassy $Pr_{60}Fe_{30}Al_{10}$ alloy, together with remanence magnetization values ~1 kG, maximum energy product ~3 MG Oe and Curie temperatures ~275 °C. Such unexpected high coercivity was explained in terms of a homogenous dispersion of exchange-coupled Nd–Fe and Nd–Fe–Al clusters with large random magnetic anisotropy, which presumably develop within the cast bulk alloys as a consequence of a relaxed disordered atomic configuration, afforded by the slow cooling rate characteristic of the mold cast process [4,5]. The exchange coupling interaction in amorphous Nd–Fe–Al alloys has been confirmed through the observation of magnetic domains of an average length of 360 nm by means of MFM [6]. Further HRTEM and radial distribution studies have estimated the cluster size as 2 nm on average [7–9].

In contrast, several authors [10–15] have described composite Nd–Fe–Al alloys rather than single-phase amorphous alloys. In general, these RE–TM–Al-based composite structures have been reported as comprising nanosized Nd-rich crystallites embedded within an amorphous matrix. The crystalline phase forms an extended network over the whole sample with a small volume fraction, presumably lower than 5–6% and thus, just below the X-ray diffraction limit detection. Therefore, the correlation coercivity–amorphous/crystalline volume fraction can be monitored by careful heat treatments. For example, diminishing coercivity values were observed in $Nd_{70}Fe_{20}Al_{10}$ alloys for increasing annealing temperatures (from 50 to 450 °C), which was attributed to the increasing size of the Nd precipitates [14]. Alternative approaches consider a pinning model for domain walls between magnetic domains [16,17], for which the nanosized Nd-rich crystallites act as pining centers, thus hindering the domain wall displacement and hence, giving rise to the high coercive field characteristic of (Nd,Pr)–Fe–Al bulk alloys. In this work, we study

* Corresponding author. Fax: +52 56161371.
E-mail address: raorze@hotmail.com (R.Ortega-Zempoalteca).

0925-8388/$ – see front matter © 2010 Elsevier B.V. All rights reserved.
doi:10.1016/j.jallcom.2010.04.255

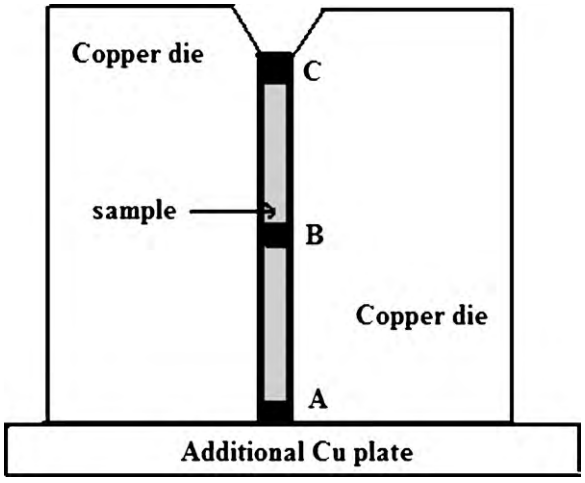

Fig. 1. Experimental set-up for die-casting process of the $Nd_{60}Fe_{30}Al_{10}$ alloy. The labels A, B and C indicate the samples selected from the rod.

the magnetic property dependence with the amorphous/crystalline volume fraction within a single rod of bulk composite $Nd_{60}Fe_{30}Al_{10}$ alloys.

2. Experimental techniques

A master alloy ingot with composition $Nd_{60}Fe_{30}Al_{10}$ was prepared by arc-melting the pure component elements within inert Ar atmosphere. An individual cylindrical rod (3 mm diameter and 50 mm length) was obtained from the master alloy by means of die-casting process into a copper mold under inert atmosphere. For the casting procedure, the metallic mold was located on an extra copper block, as indicated in Fig. 1. From the obtained metallic cylinder, three different cutting zones were selected for sampling: zone A for the bottom part (in direct contact with the additional Cu plate), zone B at the middle and zone C for the upper portion of the alloy rod (i.e. at the open side of the copper mold), Fig. 1. The microstructure of the as-cast alloy sample was characterized by X-ray diffraction analysis, XRD (Bruker-AXS D8, with Cu-Kα radiation) and by Transmission Electron Microscopy, TEM (Jeol 1200EX operating at 120 kV). On the other hand, room temperature magnetic measurements (maximum magnetization M_{max}, remanence magnetization M_r and intrinsic coercivity H_c) were carried out by means of a Vibrating Sample Magnetometer VSM (LDJ 9600) with a maximum applied field of 1360 kA/m, while the Curie temperature T_c was determined using Magnetic Thermogravimetric Analysis (MTGA) on a TA instruments 2950 thermobalance with a heating rate of 10 K/min and coupled with a permanent magnet.

3. Results

X-ray diffractograms for samples A, B and C are shown in Fig. 2. The single broad maximum manifested for sample A at low 2θ angles is consistent with a majority amorphous phase (relative to the XRD detection limit). In contrast, for sample B, some broad peaks at $2\theta = 28.4^\circ$ corresponding to (1 0 0) planes of hcp-Nd, and $2\theta = 47.7^\circ$, 55.9°, associated to (2 2 6) and (9 0 4) planes, respectively, of the hexagonal Nd_5Fe_{17} phase are indicative of a progressive crystallization process. For sample C, all of these peaks display enhanced intensities, together with additional maxima at $2\theta = 32.3^\circ$ and 42.2° of the same phases. This phase distribution is in agreement with previous reports on equivalent Nd–Fe–Al bulk alloys [18]. The increasing crystallized state along the rod length is supported by the TEM micrographs displayed in Fig. 3, for which an initial composite structure comprising a predominant amorphous phase with some precipitates smaller than 50 nm are observed for zone A in Fig. 3a, with the corresponding diffraction pattern DP exhibiting some few spots immersed in diffuse haloes. For sample B (Fig. 3b), larger crystals are evident alongside a DP including more defined ring-like shape overlapped with diffuse haloes. Finally, for sample C, it was possible to find mostly crystallized zones with minor amorphous areas, as it is illustrated in Fig. 3c and the associated DP. Additionally, DSC scans for cutting zones A, B and C are displayed in Fig. 4, for which the crystallization temperature T_x is located at 500 °C for all the samples, while their melting onset T_m can be established at 645 °C. In addition, a decreasing heat of crystallization ΔH_{crys} is also noticeable for the sequence $\Delta H^A_{crys} > \Delta H^B_{crys} > \Delta H^C_{crys}$ (15.9, 13.6 and 5.4 J/g, respectively).

On the other hand, the M–H curves corresponding to A, B and C cuts are shown in Fig. 5. For zone A, a wide hysteresis loop with a demagnetizing quadrant with good squareness is observed, with the following associated magnetic properties: intrinsic coercivity, H_c, of 3519 Oe, remanence magnetization, M_r, of 14.5 emu/g and maximum magnetization, M_{max}, of 20.8 emu/g. Same coercivity and remanence are visible for sample B, but with a noticeable step on the second quadrant and a slightly enhanced M_{max} of 22.1 emu/g. In contrast, for sample C, a clear different magnetization curve was recorded, characterized by a poor squareness on its second quadrant, together with diminished H_c and M_r of 3070 Oe and 12.1 emu/g, respectively, but a constant M_{max} value (relative to zone B). Additionally, the Curie temperature of the amorphous phase for all alloy samples resulted of 189 °C according to MTGA experiments, as it is illustrated in Fig. 6 for cut A sample, which displays the expected "weight loss" as a consequence of the nil attraction between the permanent magnet and the sample at the ferromagnetic–paramagnetic T_c point.

4. Discussion

The microstructure of the sample A can be described as having a predominant amorphous phase with a minor distribution of fine paramagnetic Nd nanoparticles, as it is suggested by Figs. 2 and 3. Equivalent microstructure features for Nd–Fe–Al bulk alloys have been reported in Refs. [16,17,12]. A progressive diminishing amorphous fraction was observed for the cutting zones B and C, as suggested by their corresponding DSC scans (Fig. 4), which reflect an increasing crystalline volume fraction from A to C as indicated by the decreasing heats of crystallization, which are consistent with a reduced amorphous volume fraction being transformed upon heating. The composition of the ferromagnetic glassy phase should be the same for all the samples, since their Curie temperatures as well as their crystallization temperatures remain constant for all the alloy samples. The increasing crystalline volume fraction within the same alloy rod can be explained in terms of a more efficient heat transfer at the bottom of the copper mold (zone A), afforded

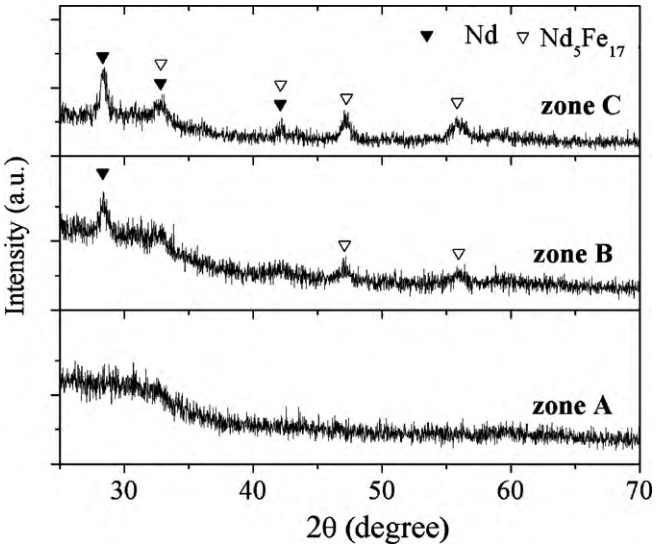

Fig. 2. X-ray diffractograms for samples A, B and C of the $Nd_{60}Fe_{30}Al_{10}$ alloy rod. The reflections of crystalline hcp-Nd and Nd_5Fe_{17} phases are indicated.

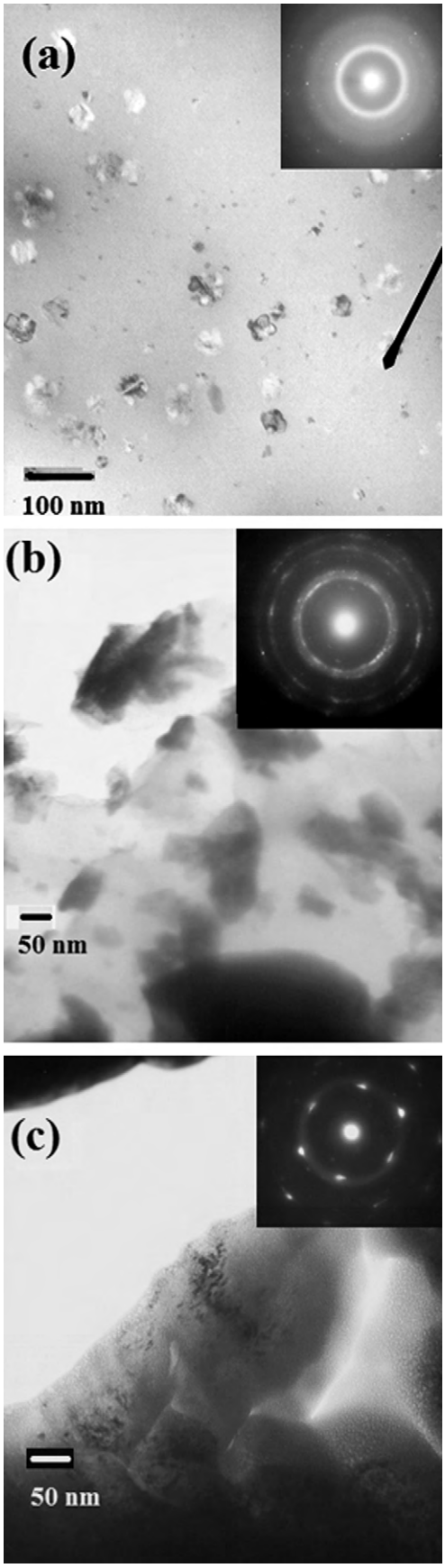

Fig. 3. TEM micrographs showing microstructure variations for the cutting zones A, B and C of the $Nd_{60}Fe_{30}Al_{10}$ alloy rod. The corresponding electron diffraction patterns are shown in the insets.

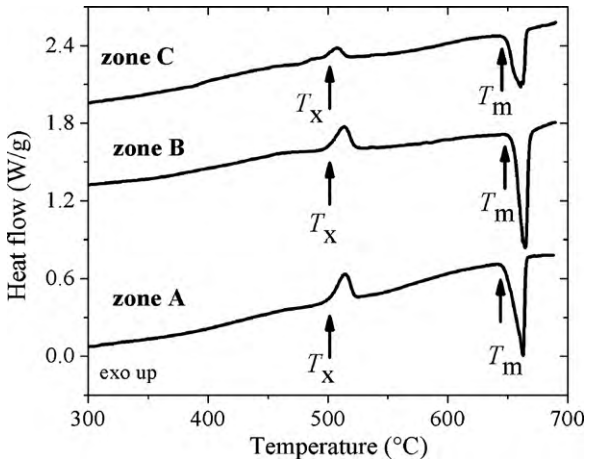

Fig. 4. DSC scans for the A, B and C zones of the $Nd_{60}Fe_{30}Al_{10}$ alloy rod. The corresponding crystallization temperature T_x at 500 °C and melting temperature T_m at 645 °C are indicated.

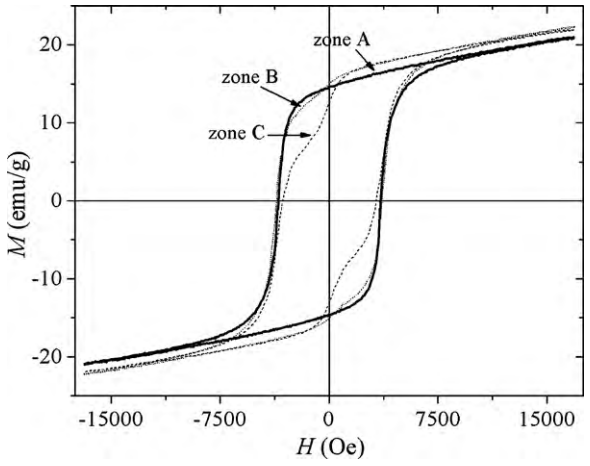

Fig. 5. *M–H* curves of samples A, B and C of the $Nd_{60}Fe_{30}Al_{10}$ alloy rod.

by the additional metallic plate used to place the die, which in turn allows a higher cooling rate compared with samples B and C, for which a less efficient heat dissipation facilitates the nucleation and further crystallization of significant portions of these alloy zone.

Concerning the magnetic properties, they are also congruent with a composite microstructure with variable crys-

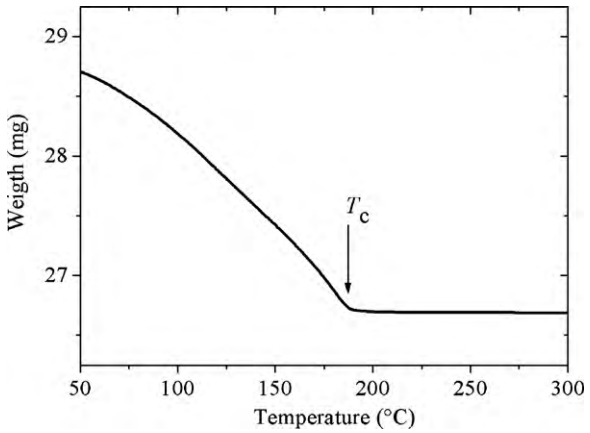

Fig. 6. MTGA curve corresponding to cutting zone A of the $Nd_{60}Fe_{30}Al_{10}$ alloy rod showing the ferromagnetic–paramagnetic transition temperature T_c.

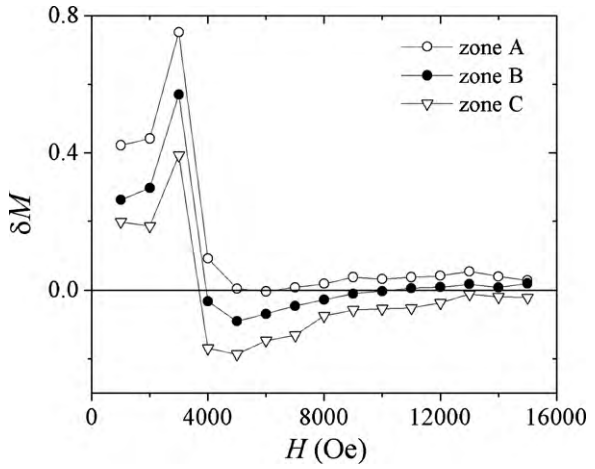

Fig. 7. Henkel plots $\delta M(H)$ for samples A, B and C of the $Nd_{60}Fe_{30}Al_{10}$ alloy rod. Solid lines are only a guide for the eye.

talline/amorphous volume fractions. For instance, the M–H loop of sample A shown in Fig. 5 with a smooth demagnetizing second quadrant is indicative of a magnetically coupled composite microstructure, for which the minority crystalline secondary precipitates contribute to the alloy coercivity through the pinning mechanism described in detail in [16,17].

In contrast, the shallow step observed for sample B would be a consequence of the increasing precipitation of the secondary crystalline phases which lead to a magnetic decoupling effect among ferromagnetic amorphous areas and crystalline phases. This decoupling effect resulting from increasingly isolated ferromagnetic zones becomes more noticeable for sample C, as evidenced by the shoulder on the second quadrant of its M–H plot, besides the discernible reduction in H_c. This picture of decreasing magnetic coupling for the sample sequence A > B > C is supported by the Henkel plots $\delta M(H)$ shown in Fig. 7, for which the positive portion of δM is usually associated with a predominant magnetic interaction of exchange coupling character between magnetic phases, whereas the negative section of $\delta M(H)$ is indicative of the prevalence of the dipolar interaction [19–21]. For sample A, the prevalent positive portion of its δM curve reflects a prime exchange coupling interaction between ferromagnetic areas which are in close proximity, whereas for samples B and C, the progressive isolation between such ferromagnetic zones (due to the increasing presence of secondary crystalline phases) provokes the preponderance of the negative portion of the δM curves.

5. Conclusions

The microstructure for an individual die-cast $Nd_{60}Fe_{30}Al_{10}$ cylindrical alloy shows significant variations along its longitudinal axis, which largely influence its magnetic properties. Optimal microstructure for maximum coercivity (3519 Oe) was observed for the bottom section of the alloy rod, for which an efficient heat transfer during the die-cast process can be expected.

Acknowledgments

The authors are grateful to G. Lara, O. Novelo, E. Fragoso and C. Flores for their valuable technical assistance during the alloy sample preparation and characterization. This work was partially supported by grant IN113908 from PAPIIT-DGAPA-UNAM.

References

[1] Y. He, S.J. Poon, G.J. Shiflet, Science 241 (1988) 1640.
[2] A. Inoue, K. Ohtera, A.P. Tsai, T. Masumoto, Jpn. J. Appl. Phys. 27 (1988) L479.
[3] Y. He, C.E. Price, S.J. Poon, G.J. Shiflet, Philos. Magn. Lett. 70 (1994) 371.
[4] A. Inoue, T. Zhang, W. Zhang, A. Takeuchi, Mater. Trans. JIM 37 (1996) 99.
[5] A. Inoue, T. Zhang, A. Takeuchi, Mater. Trans. JIM 37 (1996) 1731.
[6] B.C. Wei, W.H. Wang, M.X. Pan, B.S. Han, Z.R. Zhang, W.R. Hu, Phys. Rev. B 64 (2001) 012406.
[7] P. Min Xiang, W. Bing Chen, X. Lei, W. Weihua, Z. Dequian, Z. Zhi, H. Bao Shan, Intermetallics 10 (2002) 1215.
[8] A. Inoue, A. Takeuchi, T. Zhang, Metall. Mater. Trans. A 29A (1998) 1779.
[9] L.Q. Xing, J. Eckert, W. Löser, S. Roth, L. Schultz, J. Appl. Phys. 88 (2000) 3565.
[10] Z.G. Sun, W. Löser, J. Eckert, K.H. Müller, L. Schultz, J. Magn. Magn. Mater. 261 (2003) 122.
[11] N.H. Dan, N.X. Phuc, N.M. Hong, J. Ding, D. Givord, J. Magn. Magn. Mater. 226–230 (2001) 1385.
[12] S. Schneider, A. Bracchi, K. Samwer, M. Seibt, P. Thiyagarajan, Appl. Phys. Lett. 80 (2002) 1749.
[13] G. Kumar, J. Eckert, W. Löser, S. Roth, L. Schultz, Scr. Mater. 48 (2003) 321.
[14] E. Olivetti, M. Baricco, E. Ferrara, P. Tiberto, L. Martino, J. Magn. Magn. Mater. 290–291 (2005) 1214.
[15] G. Kumar, J. Eckert, L. Schultz, S. Ram, Mater. Lett. 53 (2002) 305.
[16] R. Sato Turtelli, D. Triyono, R. Grossinger, H. Michor, J.H. Espina, J.P. Sinnecker, H. Sassik, J. Eckert, G. Kumar, Z.G. Sun, G.J. Fan, Phys. Rev. B 66 (2002) 054441.
[17] R. Ortega-Zempoalteca, I. Betancourt, R. Valenzuela, J. Magn. Magn. Magn 321 (2009) 3159.
[18] M.J. Kramer, A.S. OïConnor, K. W: Dennis, R.W. McCallum, L.H. Lewis, L.D. Tung, N.P. Duong, IEEE Trans. Magn. 37 (2001) 2497.
[19] G. Bertotti, Hysteresis in Magnetism, Academic Press, San Diego, 1998, p. 250.
[20] J. Garcia-Otero, M. Porto, J. Rivas, J. Appl. Phys. 87 (2000) 7376.
[21] W. Liu, Y. Liu, R. Skomski, D.J. Sellmyer, Nanostructured exchange-coupled magnets, in: Y. Liu, D. Sellmyer, D. Shindo (Eds.), Handbook of Advanced Magnetic Materials, Tsinghua University Press, Springer, New York, Beijing, 2006, p. 226.